arXiv:astro-ph/9705018v1 5 May 1997

The ROSAT bright source RX J0222.4+4729 : an active nearby short-period binary of the BY Dra type [⋆]

Claude Chevalier and Sergio A. Ilovaisky

Observatoire de Haute-Provence (CNRS), F-04870 St.Michel l'Observatoire, France

Abstract. We report the discovery of a new BY Dra-type binary identified as the optical counterpart of the bright source RX J0222.4+4729 detected during the ROSAT All-Sky Survey (Voges et al. 1996). The star is a $V \sim 11.1$, near-by (~ 30 pc), close spectroscopic binary with an orbital period $P = 0.46543 \pm 0.00001$ d. The absorption-line radial velocities were obtained at the 1.93-m Haute-Provence (OHP) telescope with the *Elodie* echelle spectrograph by on-line numerical cross-correlation.

The M0Ve primary exhibits strong Balmer and Ca II H+K line emission, placing this system amongst the most active BY Dra stars. The width of the cross-correlation function yields a projected rotational velocity of $v \sin i \sim$ 85 km/s. While only the primary contributes to the continuum and the absorption line spectrum, the dM5e secondary is detected through its Hα emission. The mass ratio, estimated from the amplitudes of the emission radial velocity curves, is $q = M_2/M_1 \sim 0.4$.

CCD photometry in the B and V bands, obtained with the OHP 1.2–m and 0.80–m telescopes, shows that the optical flux is modulated at the spectroscopic period with a total amplitude of 0.2 mag and little or no color change in $B - V$. The light curve, which can be attributed to rotational modulation of the synchronized active primary star, shows extrema near quadratures and also exhibits long-term variations in average brightness (by 0.1 mag), which are accompanied by changes around the photometric minimum. A secondary minimum appears at phase 0.5, indicating a partial eclipse of the primary star.

In contrast with many other BY Dra systems, the equivalent width of the Hα emission from the RX J0222.4+4729 primary is directly correlated with photospheric brightness, *i.e.* maxima and minima occur around the same phases in both curves. However, the minimum at mid-phase in the Hα equivalent width is broader and deeper than the V-band minimum at $\phi = 0.5$ and appears shifted towards phase 0.45, suggesting that Hα emission comes from extended regions connecting the main starspot groups.

We find an X-ray to bolometric luminosity ratio of $\log(L_x/L_{bol}) \sim -3.1 \pm 0.14$ which supports the concept of saturation of coronal X-ray emission for the most rapidly rotating late-type stars.

Key words: stars: activity – stars: starspots – binaries: spectroscopic – X-rays: stars

1. Introduction

As part of an identification program of X-ray sources discovered near the galactic plane during the ROSAT All-Sky Survey (Voges et al. 1996), we present here the results of the optical identification and follow-up observations of the bright source RX J0222.4+4729. The star identified with this source is shown to be an active binary of the BY Dra type with one of the shortest (if not the shortest) orbital periods.
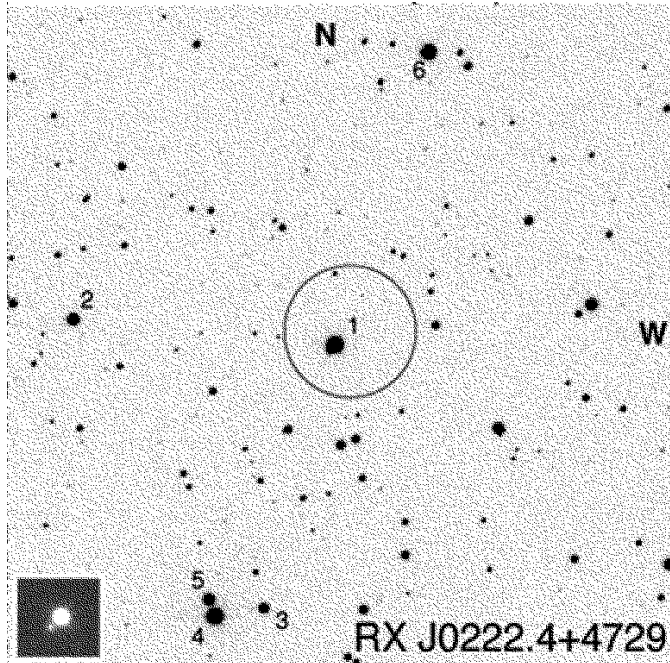
2. Optical identification

2.1. Photometric observations

CCD photometry was obtained at Haute-Provence Observatory with the 0.8–m and 1.2–m telescopes. On the 0.8–m telescope we used the RCA No.3 CCD camera, equipped with a thinned, back-illuminated 512×323 chip with 30 μ pixels, yielding at the f/15 Cassegrain focus a 2.2×3.5 arc–min field of view with a projected pixel size of 0.41 arc–sec. On the 1.2–m telescope we used the TK512 No.2 CCD camera, equipped with a thinned, back-illuminated, AR-coated Tektronix 512×512 chip with 27μ pixels, giving at the f/6 Newton focus a 6.5×6.5 arc–min field of view with a 0.77 arc–sec projected pixel size. Data were obtained on 1993 November, on 1994 November and December and on 1995 September and October. See

---

Table 1 for the observing log. The CCD images were reduced within the MIDAS environment following standard procedures. Small aperture photometry (allowing for pixels lying partly within the aperture) was used to perform relative measurements. The differential magnitudes were computed with an aperture radius less than or equal to the stellar FWHM. On frames used for calibration a growth-curve method (Howell 1989, Stetson 1990) was applied to stars without close neighbours in their profile wings, yielding the average correction needed to convert the small aperture measurements into magnitudes integrated over the entire stellar profile.

25.98s, $\delta_{2000} = +47° 29' 17.9"$ as derived from the Digitized Sky Survey CD-ROM set. This position should be accurate to $\pm0.6"$ r.m.s. (Véron-Cetty and Véron 1996).
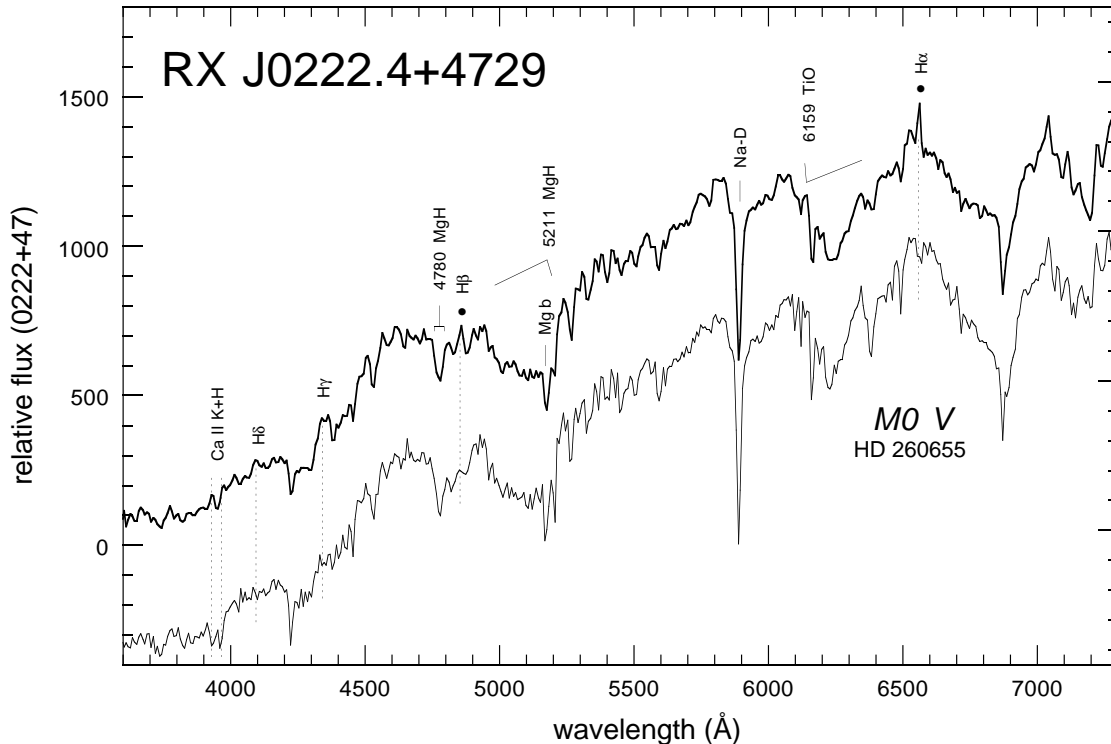
Table 1. Photometry Log

Date	Telescope	No. of Exp.	Filter
1993 Nov 11-12	0.8m OHP	43	V
1993 Nov 12-13	"	70	"
1993 Nov 13-14	"	39	"
1993 Nov 14-15	"	55	"
1993 Nov 16-17	"	44	"
1993 Nov 17-18	"	35	"
1993 Nov 19-20	"	15	"
1993 Nov 20-21	"	29	"
1993 Nov 21-22	"	19	"
1994 Nov 15-16	1.2m OHP	50	V
1994 Nov 25-26	"	27	"
1994 Dec 11-12	"	16	"
1994 Dec 13-14	"	46	"
1994 Dec 14-15	"	46	"
1995 Sep 13-14	1.2m OHP	17	B,V,R,I
1995 Sep 14-15	"	26	B,V
1995 Sep 15-16	"	32	B,V
1995 Sep 17-18	"	26	B,V
1995 Oct 12-13	"	10	B,V
1995 Oct 15-16	"	15	V
1995 Oct 16-17	"	12	V

Fig. 1. Finding chart for RX J0222.4+4729 made from a V–band CCD image taken at the OHP 1.2–m telescope. The preliminary 90% confidence error circle of 40" radius is shown centered at the ROSAT X-ray position. The bright star within the circle is the proposed $V = 11$ optical counterpart, called Star 1. Stars 2 to 6 were used as comparison and check stars. The magnitudes and colors of the numbered stars are given in Table 2. The inset frame at the lower left is a close-up view of the area around Star 1 obtained from a CCD frame taken at the 0.8–m telescope and displayed at twice the scale to show the $V = 15.1$ neighbor at 4.5" SE of Star 1.

2.2. Low-resolution spectroscopy

A low-dispersion spectrum of Star 1 was obtained on the night of 1991 October 7/8 using the *Carelec* spectrograph (Lemaitre et al. 1990) at the Cassegrain focus of the Haute-Provence 1.93–m telescope, equipped with a thinned, back-illuminated CCD (RCA No.1) having 323×512 pixels of 30 μ. A 5-min exposure was taken using a 260 Å/mm grating with a projected slit width of 2.4 arc–sec, yielding an effective resolution of 15 Å FWHM and covering the wavelength range 3500-7300 Å. Wavelength calibration was done using a He–Ar lamp and flat-fielding using an internal Tungsten lamp. The standard star Feige 25 was observed later in the night and was used to derive a relative flux-calibrated spectrum for our candidate. All reductions were made using the Spectroscopy package in MIDAS.

The relative flux distribution of Star 1 in the wavelength interval $\lambda\lambda$ 3520-7340 Å is shown in Figure 2, together with the spectrum of the M0V star HD 260655 extracted from the atlas of Jacoby et al. (1984). The continuum and the absorption lines are almost identical in the two spectra, which classifies Star 1 as a dwarf of spec-

Figure 1 is a finding chart for the RX J0222.4+4729 field made from a 1.2–m CCD frame. The 90% confidence 40" radius ROSAT error box of RX J0222.4+4729 contains an 11th magnitude star (GSC 3298.01172, Star 1 in Figure 1) lying about 13" SE from the X-ray position given in the ROSAT All-Sky Bright Source Catalog (Voges et al. 1996) where the total positional error is listed as $\pm8"$. The optical astrometric position for Star 1 is : $\alpha_{2000} = 02h 22m$

Fig. 2. The relative flux distribution of RX J0222.4+4729 (Star 1) in the wavelength range $\lambda\lambda$ 3520-7340 Å, obtained with *Carelec*, is shown together with the spectrum of the M0V star HD260655 (shown with a vertical offset) extracted from the atlas of Jacoby et al. (1984). The continuum and the absorption lines are similar in the two spectra with the noticeable exception of the Balmer lines and the Ca II H+K lines which appear in emission in the spectrum of Star 1.

tral type M0. Moreover, the presence of Balmer and Ca II H+K emission lines is the signature of chromospheric activity and strongly suggests that Star 1 is the optical counterpart of RX J0222.4+4729. The optical variability and binarity which we found (see later) further classify this object as a BY Dra binary.

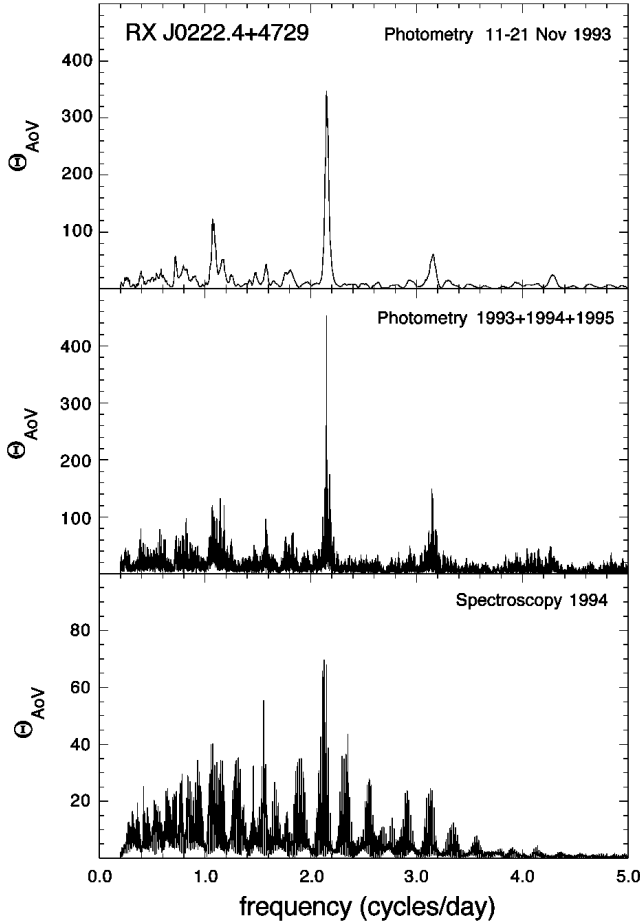### 2.3. Average Magnitude, Colours, Distance and X–Ray Luminosity

CCD frames in the Cousins B, V, R, I bands were obtained during one hour around the meridian on 1995 September 13, when seeing was poor due to strong winds but weather conditions were photometric, useful for measuring the magnitudes of the bright stars of Figure 1 with the exception of Star 5 which was measured on September 15 with better seeing but only through B and V filters.

The instrumental magnitudes were transformed to Cousins magnitudes using previous calibrations of our equipment (telescope+camera+filters) and using extinction coefficients determined during nights of similar weather conditions. The resulting uncertainty on the zero point is difficult to evaluate, but our Cousins magnitudes and colours are probably accurate to a few percent. The average V magnitude and colours obtained in 1995

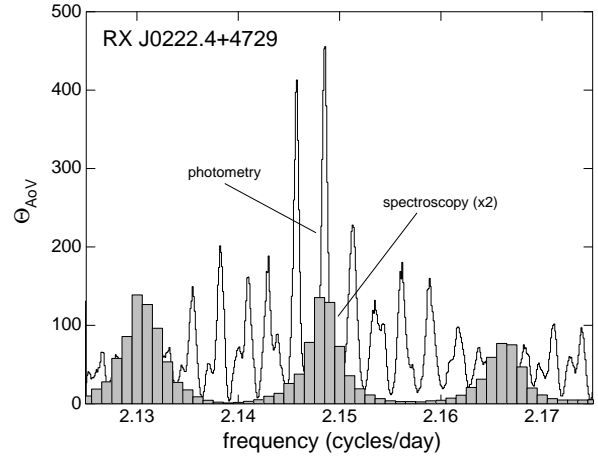**Table 2.** Average magnitudes and colours for the stars in Figure 1 (1995 September)

Star No.	V	$B - V$	$V - R_c$	$V - I_c$
1 (0222.4+4729)	11.10	1.44	0.89	1.74
2	12.80	0.43	0.28	0.55
3	13.60	0.41	0.28	0.54
4	11.05	0.43	0.28	0.54
5	12.96	0.94		
6	11.65	0.72	0.42	0.79

September for RX J0222.4+4729 (Star 1) and for the comparison stars (2 to 6) are given in Table 2. The inset frame at the bottom of Figure 1 was obtained with the 0.8-m telescope (at f/15) and shows the surroundings of Star 1 at twice the scale of Figure 1. The V magnitude of the nearby star at about 4.5 arc–seconds SE of the counterpart was measured using the PSF-fitting routine NSTAR of DAOPHOT (Stetson 1987) on several frames obtained on 1993 November 13 and is equal to $V = 15.1$ (internal dispersion ±0.06 mag). This faint neighbour does not introduce errors larger than a few mmag in the differential photometry of Star 1 through apertures of radius smaller than 3 arc–seconds.

Fig. 3. AoV periodograms obtained by phase–binning of three data sets : **Top (a)** Differential V–band 0.8–m CCD photometry (349 data points) obtained on 1993 November 11-21 (computed with a frequency step of 0.004 cycles/day). **Middle (b)** The complete V–band photometry data set (615 data points) obtained in 1993, 1994 and 1995 (computed with a frequency step of 0.0005 cycles/day). The 1993 data have been shifted by 0.1 mag to compensate for the variations in average brightness between 1993 and 1994+1995. **Bottom (c)** Radial velocities of the metallic absorption lines (38 data points obtained in October and December 1994) (computed with a frequency step of 0.001 cycles/day).

Between 1993 November to 1995 October, the V magnitude of Star 1 varied between 11.0 and 11.3 (see later the discussion on variability). Assuming M_v in the range 8.5–9 (Allen 1973, Gray 1992), corresponding to the spectral type M0V, yields a distance in the range 25-35 parsecs for the optical counterpart of RX J0222.4+4729. The ROSAT counting rate of 0.221 ± 0.022 c/s and hardness ratio HR1 $= 0.06 \pm 0.09$ (Voges et al. 1996) give a 0.1-2.4 keV flux of 1.9×10^{-12} erg cm^{-2} s^{-1}, (using the conversion relation given by Fleming et al. 1995a), which yields an X-ray luminosity of 1.9×10^{29} erg s^{-1} for a distance of 30 pc, assuming negligible interstellar absorp-

Fig. 4. The periodogram of Figure 3b has been recomputed with a higher frequency resolution (0.0001 cycles/day) in the interval 2.125-2.175 cycles/day and is plotted together with the corresponding part of the radial velocity periodogram of Figure 3c.
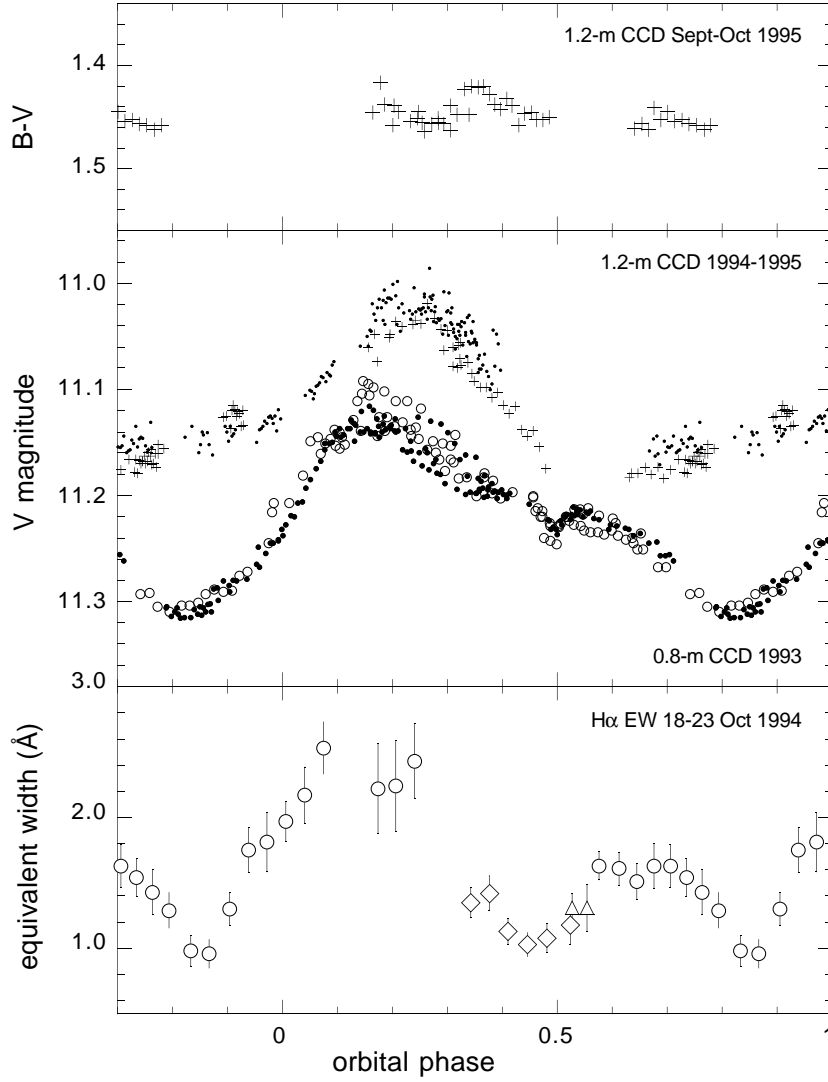
tion. For $L_{bol} = 2.6 \times 10^{32}$ erg s^{-1} (Allen 1973, Pettersen 1983) we obtain an X-ray to bolometric luminosity ratio of $\log(L_x/L_{bol}) = -3.1 \pm 0.14$. Results from the *Einstein*, EXOSAT and ROSAT soft X-ray surveys (Fleming et al. 1989, 1995b; Pallavicini et al. 1990; Schmitt et al. 1995) show that all K and M dwarf stars with Balmer emission have X-ray luminosities in the range $10^{27} - 10^{30}$ erg s^{-1} and that for M dwarfs $\log(L_x/L_{bol}) \simeq -3$, in agreement with the above determination.

This BY Dra binary close to the center of the error box is thus sufficient to account for the observed X-ray flux without having to consider the contribution from any other possible X-ray sources in the error box.

3. Photometric variability

3.1. Time analysis of photometric data

The 1993 November photometry was done differentially with respect to comparison stars 4 and 3 marked on Figure 1 and restricted to the V band. Our period search on this data set, containing 349 ΔV points, used the Analysis of Variance (AoV) method (Schwarzenberg-Czerny 1989) as implemented in the MIDAS Time-Analysis package. This method is based on phase binning and does not make any prior assumption concerning the shape of the light curve. The variance statistic Θ was computed with a frequency step of 0.004 c/d and 6 bins. The resulting periodogram (Figure 3a) is unambiguous. A strong ($\Theta = 350$) peak is present at a frequency close to 2.150 c/d, corresponding to a period of 0.465 d, accompanied by smaller ones at half the main frequency ($\Theta = 120$), at 3.15 c/d (a 1-day alias with $\Theta = 60$) and at twice the main frequency ($\Theta = 30$). The photometric data acquired in 1994 November and December (185 ΔV data points)

Fig. 5. Top (a) The $B - V$ light curve obtained in 1995 (crosses) is plotted (crosses) as a function of the orbital phase (using the same ephemeris as for Figure 6) and shows no significant variation for a V change from 11.0 to 11.17. **Middle (b)** The V–band light curve obtained in 1993 (split in two parts : 11-14 November 1993 (filled circles) and 16,19-21 November 1993 (open circles)), 1994 (dots) and 1995 (crosses) is plotted as a function of the orbital phase. **Bottom (c)** The equivalent width EW1 of the Hα_1 line (emitted by the primary M0V star) is plotted as a function of the orbital phase (open circles: 18 October, open triangles: 21 October and open diamonds: 23 October).

and in 1995 September and October (81 ΔV data points) were then added to the 1993 ΔV data set with a shift of 0.1 mag to compensate for the variation in average brightness of the source between 1993 and 1994–1995. The AoV periodogram on the whole data set (615 ΔV data points) was computed with a frequency step of 0.0005 c/d and 6 bins and is shown in Figure 3b, confirming the peak of Figure 3a.

To refine the determination of the peak frequency, we analyzed the frequency interval 2.125-2.175 c/d at the higher resolution of 0.0001 c/d. The resulting AoV periodogram, shown in Figure 4, exhibits a maximum $\Theta = 450$ at a frequency 2.14855 c/d corresponding to a period

$P = 0.46543 \pm 0.00002$ d. This period, also found in the radial velocity variations of Star 1 (which demonstrate the binary character of the system –see next Section) is hence equal to the orbital period.

3.2. The light curve

While the 1993 data obtained with the 0.8-m telescope yield complete phase coverage, the 1994 and 1995 data sets, obtained with the 1.2-m telescope, have unfortunate gaps between phases 0.4 and 0.6 and around phase 0.8 (see Figure 5b). To better determine the shape of the 1993 light curve, we rejected the data points of lowest S/N and in some cases we averaged consecutive data points with

uncertainties > 0.015 mag and separated by less than 5 minutes in time. The resulting 1993 light curve of Figure 5b is plotted with filled symbols for the nights of 11, 12, 13 and 14 November 1993, and with open symbols for the five other nights (16, 17 and 19-21 November). The orbital phase was computed from the ephemeris given in Section 4 below, phase 0.0 corresponding to the inferior conjunction of the primary M0V star and phase 0.5 to its superior conjunction. Real changes of 0.02 to 0.05 mag can occur from one night to the next in the light curve shape, mostly between phases 0.1 to 0.4 around maximum light.

A minimum of depth 0.03-0.04 mag and lasting approximately 0.1 in phase is visible at phase 0.5, indicating a partial eclipse and hence a high inclination. With the exception of this shallow minimum, the light curve (as in classical BY Dra stars) can be attributed to rotational modulation of the visible star, its surface being unevenly darkened by starspots or brightened by plages, the hemisphere observed at phase 0.75 being darker than the opposite hemisphere observed at phase 0.25.

Figure 5b shows also that during the 1994 (dots) and 1995 observations (crosses), the star was 0.1 magnitude brighter on the average. The shape of the light curve was the same as in 1993 with the exception of the phase interval 0.6-1.0. where the minimum was filled in. Figure 5a shows the relative constancy of the $B-V$ color index observed in 1995 September and October.

4. High-resolution spectroscopy

4.1. Observations

38 high-resolution spectra were obtained on several nights in 1994 October and December using the *Elodie* spectrograph (Baranne et al. 1996) at the Haute-Provence 1.93–m telescope (see Table 3 for the observing log). *Elodie* is a cross-dispersed echelle spectrograph located in a temperature-controlled room and fed by optical fibers from the Cassegrain focus. A single exposure gives a spectrum, covering the interval 3906 Å to 6811 Å with a resolution of $\mathcal{R} \simeq 42000$, distributed over 67 equally-spaced orders, which is recorded on a thinned, back-illuminated 1024×1024 Tektronix CCD (TK1024 No.2). Two entrance apertures, one for the star and one for the sky, spanning each 2 arc–sec on the sky and separated by 1.8 arc–min, yield two interleaved sets of 67 orders each.

Wavelength calibration was done using a Thorium lamp and flat-fielding using a tungsten lamp, both installed in the Cassegrain adapter. The entire reduction procedure, including flat-fielding, cosmic-ray rejection, wavelength calibration and optimal extraction, is automatic and is done, immediately after the image is read out, by a pipeline software process. The observer can proceed a step further by cross-correlating the reduced spectrum, corrected to the barycenter of the solar system, with different software masks derived from Coravel-type hardware

masks (software "slots" described by two edge wavelengths for each selected line). Two such masks are normally available, F0 and K0, useful for spectral types from F0 through M0. Only metallic absorption lines are included in the masks and the radial velocities measured are those of the mean of the lines present in the spectra, normally numbering around 3000. Given the late-type spectrum of our star we used the K0 mask for all on-line reductions.

The correlation profile obtained is then displayed and an interactive fitting procedure featuring one (or two) gaussian profile(s) yields the radial velocity for the object(s) just observed. The actual uncertainty for the measured radial velocity depends on the width and depth of the cross-correlation function (CCF), and on the S/N achieved (see Queloz 1995 and Baranne et al. 1996). In a few cases where spectra were taken during bright moon conditions, when the correlation profile was affected by scattered moonlight, a correction was applied using the correlation profile derived from the sky spectrum.

The spectra of RX J0222.4+4729 were taken using exposure times ranging from 1000 to 2000 seconds, with a mean S/N ratio of 10 (at 5500 Å), but which ranged actually from 5.7 through 16, due to changes in seeing and atmospheric transparency. For our observations of RX J0222.4+4729, the expected error for a velocity determined from a S/N=10 spectrum is around 1 km/s. An experimental determination of the actual errors is given below.

While the on-line correlation process extracts the velocity information from the metallic absorption lines, individual line profiles for particular features can be examined off-line in the individual spectra. The behavior of the Hα emission profiles is reported on below. The $\lambda 6708$ Å Li I absorption line is not detected in our best signal-to-noise ratio *Elodie* spectra although it lies in the wavelength region where both the CCD and the spectrograph have a high efficiency. Also, although detected in emission on our low-resolution *Carelec* spectra (Figure 2), the Ca II H and K lines are not measurable with *Elodie*, even though they lie in the first few recorded orders. This is because the efficiency of both the CCD and the spectrograph system (including the optical fibers) are very low at these wavelengths. Much longer exposures would have been needed to achieve detection.

4.2. Radial velocity of the absorption lines

For each of the 38 spectra obtained with *Elodie*, the average radial velocity of the absorption lines was derived from the cross-correlation function (CCF) of the observed spectrum with a K0 mask. A single broad Gaussian (implying rapid rotation –see later) was always an acceptable fit to the CCF. The variability which appears in the radial velocity values listed in Table 3 clearly shows that Star 1 belongs to a binary system. The period search on this data set used also the AoV statistic, with 7 bins and a

frequency step of 0.001 c/d. The periodogram is shown in Figure 3c. The two epochs of observation separated by two months (1994 October and 1994 December) resulted in 3 equally probable peaks in the frequency interval 2.10-2.15 c/d. One of them coincides with the photometric peak as is shown in Figure 4 which is a close-up view of both photometric and radial velocity periodograms in the frequency interval 2.125-2.175 c/d. By attributing the photometric variability to rotational modulation of the M0V star, we conclude that the star's rotation is synchronized with its orbital motion, a result expected for an orbital period as short as 0.465 d.

We made a least-squares fit to obtain the best match of the radial velocities to a sine curve, starting with an initial value of $P = 0.465$ d. The four-parameter fit (period, phase, semi-amplitude and zero point), computed using the MIDAS Time-Series Analysis package, yielded a period $P = 0.46543 \pm 0.00001$ d (11.1703 hours), an epoch $T_\circ = \mathrm{HJD}\ 2449644.1042 \pm 0.0014$ for phase 0.0, where $T_\circ$ is defined as the time of an inferior conjunction of the M0V star (preceding the time of maximum redshifted velocity by 0.25 cycle), a semi-amplitude $K_1 = 66.0 \pm 0.6$ km/s and a systemic velocity $\gamma = -52.4 \pm 0.3$ km/s. The radial velocity curve of RX J0222.4+4729 is shown in Figure 6 where the radial velocities determined from the absorption lines of the M0V star spectra are plotted as open circles and the fit to a sine curve as a solid line. The goodness of the fit is an evidence for a circular orbit. The individual radial velocities are listed in Table 3 where we also give the S/N (at 5500 Å) of the spectra and the velocity residuals to the sine fit (in km/s). The standard deviation of the latter is 1.1 km/s which is close to the expected uncertainty mentioned above.

The average FWHM of the absorption-line CCF yields an estimate of the projected rotational velocity of the M0V star: $v_{rot} \sin i = 2\pi R_1 \sin i / P \simeq 85 \pm 5$ km/s, where R_1 is the M0V star radius.

4.3. The Hα emission lines

4.3.1. Radial velocity

All the *Elodie* high-resolution spectra showed strong Hα emission above the continuum. Figure 7 illustrates the profile at representative phases along an orbital cycle. At inferior (phase 0) and superior (phase 0.5) conjunctions of the primary M0V star, the Hα line showed an emission profile well matched to a single Gaussian profile, while a second component was present at intermediate phases, appearing blueward of the primary component between phases 0.1 and 0.4 and redward between phases 0.6 and 0.9. When both components were present, a bi-Gaussian fit, done off-line with the MIDAS Fitting package, yielded the central wavelengths of both components Hα$_1$ and Hα$_2$, as well as the equivalent width of the primary component above the local continuum. Given the strength of the emis-

Table 3. Absorption-line radial velocity data for RX J0222.4+4729

HJD[a]	V_{rad}[b]	ϵ[c]	ϕ_{orb}[d]	S/N[e]
(d)	(km/s)	(km/s)		
9644.3721	−81.13	+1.40	0.576	13.2
9644.3896	−95.79	−0.31	0.613	11.4
9644.4043	−104.40	+0.06	0.645	9.9
9644.4189	−113.60	−2.19	0.676	8.7
9644.4326	−116.60	−0.77	0.706	9.0
9644.4463	−118.30	−0.21	0.735	9.9
9644.4600	−117.50	+0.62	0.764	7.6
9644.4736	−114.80	+1.12	0.794	8.6
9644.4922	−109.30	+0.21	0.834	7.7
9644.5078	−103.60	−2.28	0.867	7.9
9644.5254	−87.80	+1.75	0.905	9.3
9644.5410	−73.44	+3.87	0.939	9.0
9644.5566	−64.25	−0.29	0.972	7.2
9644.5723	−48.98	+1.13	0.006	11.8
9644.5889	−36.58	−1.07	0.041	9.1
9644.6045	−22.41	+0.13	0.075	11.5
9644.6504	+2.52	−3.55	0.174	5.9
9644.6660	+12.38	+1.22	0.207	5.7
9644.6816	+14.08	+0.65	0.241	7.7
9647.6074	−63.38	+0.09	0.527	10.9
9647.6201	−75.80	−1.40	0.554	6.6
9649.3838	+3.07	+0.56	0.343	10.5
9649.3994	−6.43	−0.07	0.377	9.6
9649.4150	−18.32	−1.06	0.411	10.2
9649.4316	−32.01	−1.46	0.446	10.4
9649.4482	−42.68	+2.25	0.482	9.3
9649.4678	−58.02	+4.25	0.524	7.2
9699.3760	−119.10	−0.74	0.754	16.4
9699.5244	−20.07	+3.00	0.073	15.6
9699.5410	−9.19	+1.49	0.109	13.7
9699.5576	−3.48	−3.11	0.144	13.6
9699.5752	+7.22	−0.49	0.182	11.7
9703.3672	+3.73	−1.70	0.330	9.6
9703.3857	−2.86	+1.38	0.369	9.9
9703.4092	−21.82	−1.18	0.420	11.8
9703.4346	−41.56	+0.36	0.474	13.9
9703.5957	−114.60	−2.63	0.821	12.2
9703.6201	−100.60	−1.02	0.873	10.9

[a]　HJD–2440000 at midpoint of exposure
[b]　M0V star radial velocity of metallic absorption lines
[c]　residuals from a sine fit
[d]　using $P = 0.46543$ d and $T_\circ = 9644.1042$
[e]　at 5500 Å

sion, we have not corrected the Hα equivalent width for the underlying photospheric absorption (such a correction would add a constant term of a few tenths of an Å).

The resulting heliocentric radial velocities of Hα$_1$ and Hα$_2$ are plotted in Figure 8 as a function of the orbital phase derived from the primary absorption lines. A least-squares fit of the Hα$_1$ radial velocities to a sine curve yields the same parameters, within the uncertainties, as those de-

rived from the absorption lines: $P = 0.46540 \pm 0.00008$ d, $T_{\circ} = $ HJD 2449644.103 ± 0.004, $K_1 = 66.2 \pm 1.9$ km/s, which confirms that the Hα emission line of the primary has the same radial velocity curve as its photospheric absorption lines. Figure 8 illustrates this result, since the dotted line plotted on the Hα_1 radial velocities, which is the same sine curve plotted in Figure 6 on the absorption-line radial velocities, matches the data very well.

The fit of the Hα_2 radial velocities to a sine curve yields $P = 0.46547 \pm 0.00008$ d, $T_{\circ} = $ HJD 2449644.33 ± 0.01, $K_2 = 174 \pm 5$ km/s, adopting for Hα_2 the same systemic velocity as for the other lines, and is plotted in Figure 8 as a solid line on the Hα_2 radial velocity data (filled triangles). The radial velocity of Hα_2 varies with the same period as the radial velocities of Hα_1 and of the absorption lines but shows a phase shift of $180°$ corresponding to the difference of $P/2$ in $T_{\circ}$. We can thus assume that the radial velocities of the emission lines Hα_1 and Hα_2 reflect the orbital motion of the primary and secondary stars respectively. Although too faint to contribute to the continuum or to the absorption line spectrum, the secondary star reveals itself by the strong intensity of its Hα emission.

Assuming a mass ratio $q = M_2/M_1$ equal to the ratio of amplitudes K_1/K_2 yields $q = 0.38 \pm 0.04$. A reasonable estimate for the mass of the primary star is $M_1 = 0.52 M_{\odot}$ (Gray 1992), with an uncertainty of at least 10%. From the mass ratio q we derive for the secondary star $M_2 \sim 0.2 M_{\odot}$ (with a 20% uncertainty) which corresponds to a dwarf of spectral type M5, and $M_1 + M_2 = (0.72 \pm 0.07) M_{\odot}$

Since the primary star is more than 3 magnitudes brighter than the secondary in the Cousins R band, the continuum intensity of its spectrum around Hα should be more than 10 times brighter than the continuum intensity of the secondary and yet the Hα emission of the secondary appears above the primary's continuum at orbital phases near quadratures. We may safely conclude that the chromospheric activity of the secondary star exceeds that, already quite intense, of the primary.

4.3.2. Equivalent widths

As mentioned above, the Hα lines appear in pure emission with Gaussian profiles, indicating that the underlying photospheric absorption is relatively small. Excluding conjunction, the equivalent widths EW1 and EW2 were measured by fitting a Gaussian to each profile and a polynomial to the continuum (emitted by the primary). EW1 was found to vary between 1 and 3 Å while EW2 rarely exceeded 0.1 Å and we have neglected the contribution of EW2 to EW1 near conjunction since this contamination is small compared to the uncertainty on the placement of the local continuum.

In Figure 5c the equivalent width EW1 measured on the nights of 1994 October 18, 21 and 23 is plotted as a function of orbital phase. The EW1 modulation ap-

pears directly correlated to the 1993 V-band light curve obtained 11 months earlier (unfortunately the V light curve obtained in November and December 1994 shows too many phase gaps to be useful). Maximum EW1 occurs between phases 0.1 and 0.3 as the maximum in V; similarly a deep minimum occurs near phase 0.8 in both curves. The Hα_1 variability is apparently dominated by rotational modulation and not by flares.

Our results differ from most studies which indicate an anti-correlation of these activity tracers in BY Dra and RS Cvn stars. Such an anti-correlation is not a general rule however. Other instances of correlation are known, for example one has been observed in the single M dwarf Gliese 890 (HK Aqr) of the BY Dra type by Young et al. (1990), another one in the short-period eclipsing RS Cvn binary BH Vir (Lázaro & Arévalo 1994).

The main difference between the EW1 modulation and the V light curve is observed near the primary's superior conjunction. A deep and broad minimum in the EW1 modulation, centered near phase 0.45, corresponds to the shallow and narrow minimum at phase 0.5 in the V light curve which indicates a partial eclipse of the primary's disk. This suggests that part of the Hα_1 emission comes from co-rotating prominence-like material surrounding the primary which may be viewed off the limb, the eclipse of the prominence by the secondary occuring earlier in phase than the partial eclipse of the primary's disk.

5. Discussion

The results presented in this paper yield the orbital elements summarized in Table 4.

Table 4. Orbital elements for RX J0222.4+4729

$$K_1 = 66.0 \pm 0.6 \text{ km/s}$$
$$K_2 = 174 \pm 5 \text{ km/s}$$
$$a \sin i = (2.189 \pm 0.064) R_{\odot}$$
$$\gamma = -52.4 \pm 0.3 \text{ km/s}$$
$$(M_1 + M_2) \sin^3 i = (0.666 \pm 0.058) M_{\odot}$$
$$q \equiv M_2/M_1 = 0.38 \pm 0.04$$
$$P = 0.46543 \pm 0.00001 \text{ d}$$
$$T_{\circ} = \text{HJD } 2449644.1042 \pm 0.0014$$
$$e = 0.0$$

The rotational velocity of the primary star has been derived from the average FWHM of the cross-correlation function of its absorption lines with a K0 mask giving $v_{rot} \sin i = 2\pi R_1 \sin i / P \simeq 85 \pm 5$ km/s, where R_1 is the radius of the primary star. From this we derive $R_1/a = 0.35 \pm 0.03$ and $R_1 = 0.78 \pm 0.09 R_{\odot}$. This radius is somewhat larger than the average estimate for a main sequence M0V star but is intermediate between the radii adopted for BY Dra (M0V) and for CC Eri (K7V) (Strassmeier et al. 1993) which are both active binaries of the same type.

The grazing-incidence angle between the two stars is given by $\tan i_{graz} = 2.19/(R_1 + R_2)$, R_1 and R_2 being the radii of the primary and secondary stars respectively. Assuming for R_1 the value given above and for R_2 a value compatible with that for M_2 ($\sim 0.25\text{-}0.30 R_\odot$) gives $R_1 + R_2$ in the range 1.0-1.1 $R_\odot$ and $i_{graz} \sim 64°$. On the other hand, combining the total mass derived earlier, $M_1 + M_2 = (0.72 \pm 0.07) M_\odot$, with the value of $(M_1 + M_2) \sin^3 i$ yields an orbital inclination in the 66–90° range, with a central value of $i \sim 77°$, thus partial eclipses must occur.

At phase 0 the eclipse of the secondary is not detectable in the V light curve due to its faintness, while the minimum observed at phase 0.5 is compatible with a partial eclipse of the primary. Its shape, small depth and duration could agree with an inclination in the range $70 - 80°$. The eclipse profile may be altered by starspot groups and plages on the primary and eventually by flaring on both stars.

Considering the strength of the Balmer emission and the amplitude of the V light curve, this system is one of the most active BY Dra binaries. Variations of both the Hα emission and the V light curve are clearly dominated by rotational modulation and not by flaring. The V light curve and the Hα equivalent width of the primary are directly correlated, which is unusual among BY Dra binaries. This correlation and the minimum observed in the Hα equivalent width near the primary's partial eclipse suggest that Balmer emission occurs in large emitting loops connecting the major spot groups. The coronal X-ray emission is also a good tracer of stellar activity. For RX J0222.4+4729, a rapid rotator ($v \sin i \sim 85$ km/s), we find an X-ray to bolometric luminosity ratio of $\log(L_x/L_{bol}) \sim -3.1 \pm 0.14$. This ratio is in excellent agreement with the dependence of $\log(L_x/L_{bol})$ on projected rotational velocity derived by Stauffer et al. (1994) for Pleiades members, which shows that for $v \sin i > 15 - 20$ km/s, $\log(L_x/L_{bol})$ is constant and equal to -3. This supports the concept of saturation of coronal X-ray emission for the most rapidly rotating late-type stars, in particular for the BY Dra binaries (Pallavicini et al. 1990).
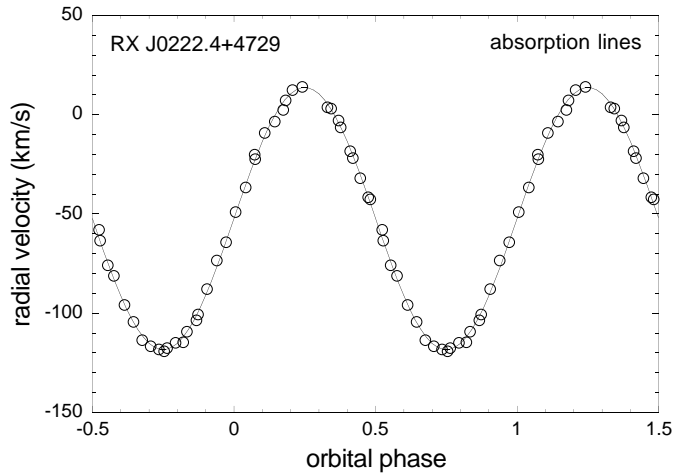
References

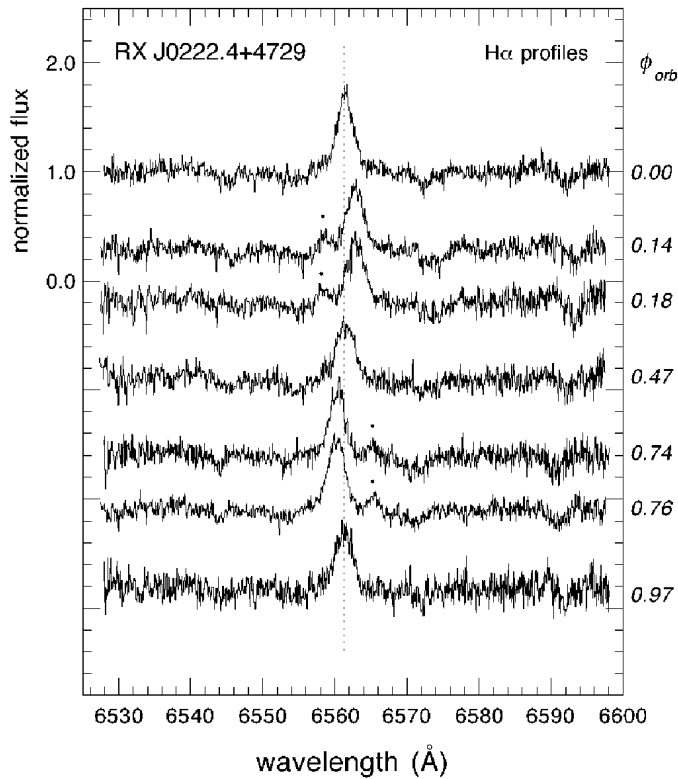Allen C.W. 1973, Astrophysical Quantities, Athlone Press, London

Baranne D., Queloz D., Mayor M., Adrianzyk G., Knispel G., Kohler D., Lacroix D., Meunier J.P., Rimbaud G., Vin A. 1996, A&AS 119, 373

Fleming T.A., Gioia I.M., Maccacaro T. 1989, ApJ 340, 1011

Fleming T.A., Molendi S., Maccacaro T., Wolter A. 1995a, ApJSS 99, 701

Fleming T.A., Schmitt J.H.M.M., Giampapa M.S. 1995b, ApJ 450, 401

Gray D.F. 1992, The Observation and Analysis of Stellar Photospheres, Cambridge University Press, Cambridge

Howell S.B. 1989, PASP 101, 616

Jacoby G.H., Hunter D.A., Christian C.A. 1984, ApJS 56, 257

Lázaro C., Arévalo M.J. 1994, Cool Stars, Stellar Systems and the Sun (8th Cambridge Workshop), J.-P. Caillault (Ed.), ASP Conf. Series, Vol.64, p. 436

Lemaitre G., Kohler D., Meunier J.P., Vin A. 1990, A&A 228, 546

Pallavicini R., Tagliaferri G., Stella L. 1990, A&A 228, 403

Pettersen B. 1983, in Activity in Red-dwarf stars, P.B. Byrne, M. Rodonò, Eds., Reidel, Dordrecht, p.17

Queloz D. 1995, IAU Symposium No. 167, New Developments in Array Technology and Applications, A.G. Davis Philip et al., Eds., Reidel, Dordrecht, p.221

Schmitt J.H.M.M., Fleming, T.A. Giampapa M.S. 1995, ApJ 450, 392

Schwarzenberg-Czerny A. 1989, MNRAS 241, 153

Stauffer J.R., Caillault J.P., Gagné M. et al. 1994, ApJS 91, 625

Stetson, P.B. 1987, PASP 99, 101

Stetson, P.B. 1990, PASP 102, 932

Strassmeier K.G., Hall D.S., Fekel F.C., Scheck M. 1993, A&AS 100, 173

Véron-Cetty M.P., Véron, P. 1996, A&AS 115, 97

Voges W., Aschenbach B., Boller Th. et al. 1996, A&AS in press

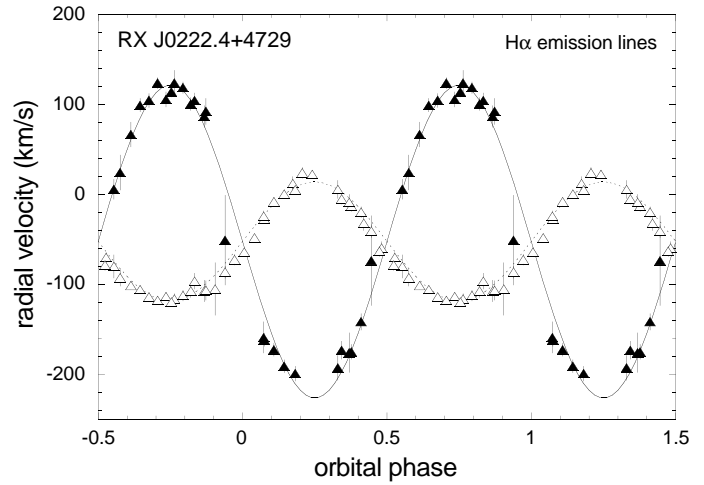Young A., Skumanich A., MacGregor K.B., Temple S. 1990, ApJ 349, 608

This article was processed by the author using Springer-Verlag LaTeX A&A style file *L-AA* version 3.

Fig. 6. The 38 radial velocity measurements for the metallic absorption lines of the M0V star in RX J0222.4+4729, obtained with *Elodie*, are plotted *vs.* the orbital phase computed from the ephemeris given in the text. $\phi = 0$ corresponds to an inferior conjunction of the M0V primary. The solid line represents a least–squares fit to a sine curve.

Fig. 7. Individual *Elodie* spectra around Hα are shown near conjunction (phases 0.0 and 0.5) and quadratures (phases 0.25 and 0.75). The Hα line emitted by the secondary star appears blueward of the primary component near phase 0.2 and redward near phase 0.7 while the profile appears single-Gaussian near phases 0.0 and 0.5. The dotted vertical line is located at the systemic velocity.

Fig. 8. The *Elodie* radial velocities of the Hα lines emitted by the primary M0V star (open triangles) and the secondary star (filled triangles) are plotted as a function of the orbital phase (computed with the same ephemeris as in Figure 5). The dotted line curve overplotted on the triangles (primary star) is the fit derived for the metallic absorption lines of the primary and shown in Figure 5.